Civil Engineering Infrastructures Journal 2025, 58(1): 123-145
DOI: 10.22059/ceij.2024.366834.1975

RESEARCH PAPER

Structural Failure of Masonry Arch Bridges Subjected to Seismic Action

Bagherzadeh Azar, A.[1*] and Sari, A.[2]

[1] Ph.D. Candidate, Institute of Earthquake Engineering and Disaster Management (ITU Graduate School), Istanbul Technical University, Istanbul, Turkey.
[2] Professor, Faculty of Civil Engineering, Istanbul Technical University, Istanbul, Turkey.

Received: 18 Oct. 2023; Revised: 04 Dec. 2023; Accepted: 25 Dec. 2023

ABSTRACT: This study investigates the seismic response of a historical arch bridge using a macro-modelling technique in Finite Element (FE) software ABAQUS. A comprehensive investigation involving documentary sources and on-site assessments has facilitated a thorough understanding of the case study, the Halilviran bridge. 3D finite element models incorporating damage plasticity behavior were constructed for the FE model. The masonry units were modelled with the Concrete Damage Plasticity (CDP) material model, and the backfill was developed with the Mohr-Coulomb (M-C) material model. Nonlinear dynamic analysis was utilized to predict the progression of damage to the bridge and determinate the most susceptible structural components. The seismic performance of the case study was evaluated through an examination of the outcomes utilizing contour plots depicting tensile damage, maximum displacements, and energy calculated from the tensile damage. The findings indicate that the spandrel walls, which are interconnected with the pier, and the inner section of the arches represent the most vulnerable components of masonry bridges, the failure of which heightens the risk of progressive collapse of the bridge.

Keywords: Masonry Arch Bridges, Seismic Behavior, Strengthening Techniques, Collapse, Bridge Failure.

1. Introduction

The breakdown of infrastructure can result in significant economic and social consequences and impede rescue and recovery efforts. It is crucial to assess the effectiveness of historical masonry structures and provide detailed and accurate data to inform maintenance decisions for reinforcing them against seismic forces.

The earthquakes that have taken place in the last 25 years have clearly shown the high vulnerability of masonry structures to seismic events (Milani, 2019b) owing to their distinctive characteristics and susceptibility to lateral forces. Research conducted post-earthquakes has shown that the main reason for the susceptibility of buildings is the presence of local failure modes, which are a result of the out-of-plane response of structural components.

Hence, it is imperative to introduce a sufficiently thorough methodology capable of accurately representing the actual structural reaction of intricate structures to lateral forces and precisely identifying the

* Corresponding author E-mail: azar19@itu.edu.tr

most vulnerable elements. Post-earthquake assessment of the structure along with Nonlinear Dynamic Analysis (NDA) is a comprehensive approach for studying the structural behavior, which involves analyzing force redistribution, ductility, damage and collapse mechanisms. Various methods have been suggested, utilizing sophisticated numerical and experimental tools to generate three-dimensional models of the structures, analyze failure mechanisms and design effective strengthening techniques (Castellazzi et al., 2017; Clementi et al., 2017; Valente and Milani, 2019). The research conducted by Li and Chen (2023) aimed to examine the seismic vulnerability of a reinforced concrete girder bridge. The investigation involved the integration of nonlinear vulnerability analysis techniques with numerical and probabilistic modeling methods. The study selected 1069 reinforced concrete bridges that had been impacted by the Wenchuan earthquake for vulnerability assessment. The vulnerability of the damaged bridges was evaluated using the Chinese seismic intensity scale. A new approach was devised to compare vulnerabilities by considering both the failure ratio and the likelihood of exceeding certain thresholds. Furthermore, a model was established to compute the average damage index of reinforced concrete girder bridges across various intensity zones. This model uses matrix calculations and compares vulnerability parameters using matrices and curves.

Li (2023) examined the seismic vulnerability characteristics of buildings and evaluates the seismic capacity of different types of structures during real seismic events. This research employed probabilistic damage model analysis techniques. Additionally, a nonlinear regression-based approach was presented for analyzing prediction models. A predictive model was created to assess structural vulnerability, taking into account failure rates and the probability of exceeding certain intensity levels in different areas. The model was validated using data from an earthquake damage database. Moreover, a vulnerability matrix predictive model was introduced, which involveed updating the mean vulnerability index parameter. A comparative model was also developed to predict the vulnerability matrix of typical structures in specific regions.

Pelà et al. (2013) performed a seismic evaluation of an existing masonry bridge consisting of three curved segments. The seismic capacity of the bridge was evaluated using time history and pushover analysis techniques. Altunısık et al. (2015) performed a research investigation on the impact of arch thickness on the load-bearing capacity of arch bridges, and evaluated the seismic resilience of such bridges. To accomplish this goal, artificial acceleration records were generated, considering the seismic characteristics of the location where the bridge is located.

Li et al. (2023) developed metrics and probability indicators to assess the resilience and vulnerability of group formations in both urban and rural settings. Their research comprised a statistical analysis of seismic damage data gathered during field surveys after the Jiuzhaigou earthquake in Sichuan Province, China. The researchers developed a methodology for comparing and analyzing multidimensional modal resilience and probability metrics. They suggested a quantitative approach to improve the precision and rationality of structural resilience evaluations in the context of macro intensity measurement. This model was based on maximizing the macro intensity index and refining the lognormal distribution. Additionally, comparative models were formulated to appraise group structure resilience against established macro intensity benchmarks. The study also encompassed on-site damage assessments and analyses of the mechanisms of destruction, considering the unique attributes of regional structural seismic resilience and the actual vulnerabilities exposed during the

earthquake event.

The current research presents the results of sophisticated numerical analyses performed on 3-D finite element models. In order to enhance the precision of evaluating the behavior of macro-elements at both local and global levels, and to qualitatively evaluate the mechanical properties of the masonry, data is incorporated from comprehensive surveys, laser scanning, and non-destructive testing.

This paper is succinctly divided into three main components. Firstly, a 3-D finite element model of the bridge is constructed. Following this, non-linear dynamic analyses are carried out, beginning with a material model. The final stage involves a detailed and meticulous analysis of the results, requiring a comprehensive understanding and significant theoretical expertise. The primary objective of the initial modeling phase is to achieve a high level of accuracy and consider various factors that significantly impact the structure's behavior in the event of a collapse. This examination encompasses several factors, including the interconnection between the spandrel walls and the condition of them, the degradation of the masonry and the stiffness of the backfill.

2. Case Study

The Halilviran Bridge is about 20 km from the city of Diyarbakir in Turkey and is located near the Devegecidi stream. The architectural composition of the bridge is made of uniform limestone. Its most important structural feature is a semi-circular arch that rises from the rocky base in both directions of the river channel.

The stone structure, consisting of seven arches, was designed to facilitate the crossing of the river obstacle. The bridge has a total length of 132 m, with a documented roadway width of 5.10 m and a height of 8.50 m above the ground. The spans of the arches range from 5.95 m to 7.00 m, increasing from west to east.

The seventh arch to the east has a special shape compared to the previous arches. It has a pointed shape that resembles the round arch, but is lower in height. Figures 1 and 2 show the architectural design, cross-sectional views and vertical views as well as the main geometric dimensions of the Halilviran bridge.

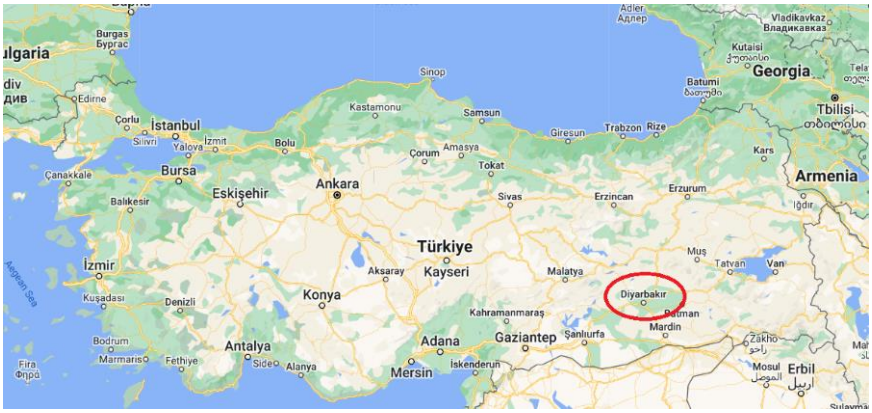

(a)

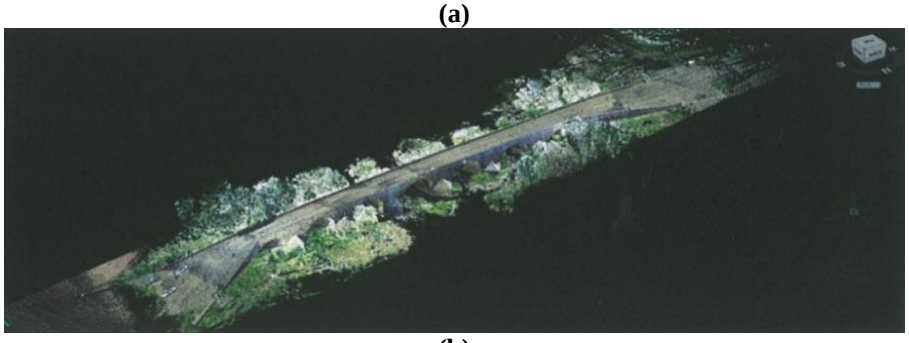

(b)

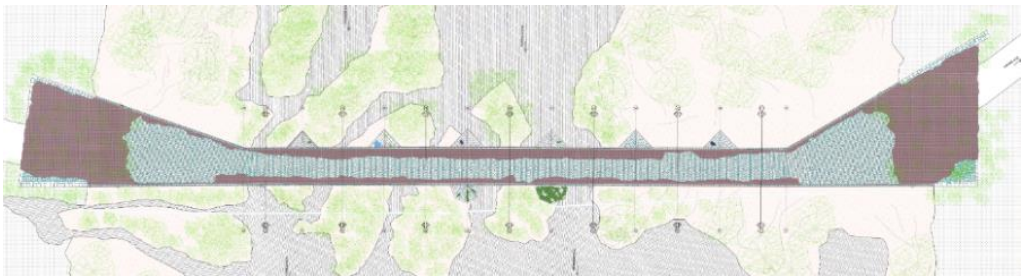

(c)

Fig. 1. Halilviran bridge: a) Location; b) 3D Scanning cloud image; and c) CAD drawing (Azar and Sari, 2023)

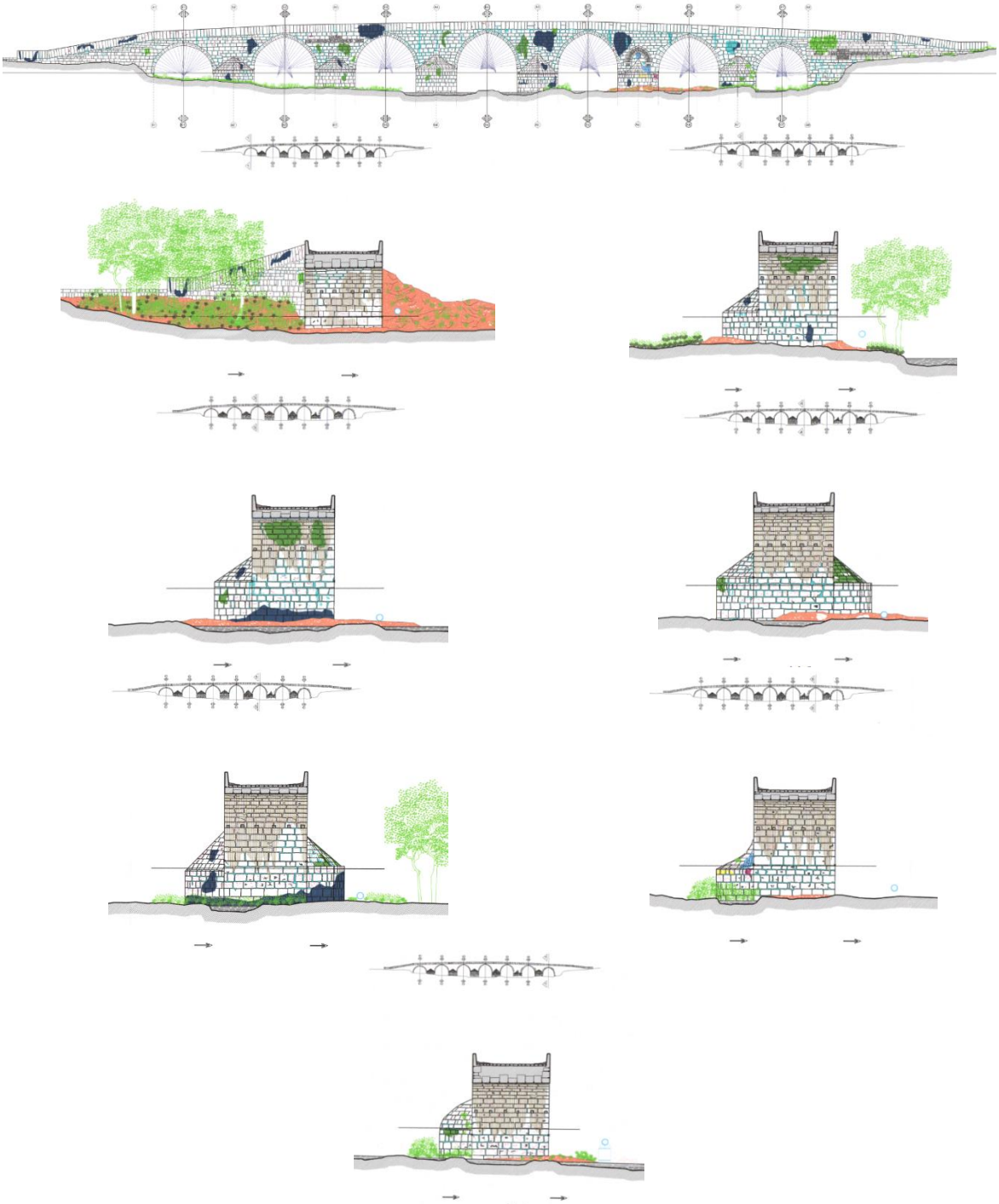

Fig. 2. Halilviran Bridge: Section and elevation views with indication of the main geometrical dimensions (Azar and Sari, 2023)

3. FE Models and Material Model Adopted

The 3D finite element discretization was applied using C3D8R, which denotes 8-node reduced integration elements. The selection of the element size was determined to achieve precise outcomes and computational effectiveness within the framework of non-linear dynamic analyses.

Figure 3 depicts the viewpoints of the geometric representations of the bridge, which were generated within the commercial software ABAQUS. These representations consist of separate structural elements known as macro-elements, as shown in Figure 4. In order to ensure the accurate modeling of the bridge's response, it is essential to consider the interplay among its different components.

This study focuses on examining the interaction between the masonry-masonry and masonry-backfill elements. The analysis assumes a zero-thickness contact, employing a hard contact model to depict the interaction between the surfaces. In this context, "hard" contact denotes an interaction where there is no softening or penetration of the surfaces within the model. Furthermore, a friction coefficient of 0.78 is adopted to characterize the tangential behavior.

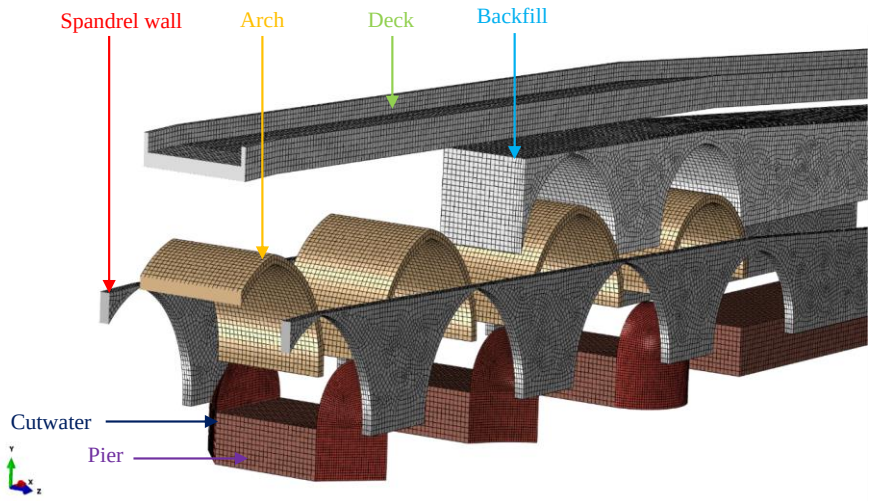

Fig. 3. Finite element model of the bridge

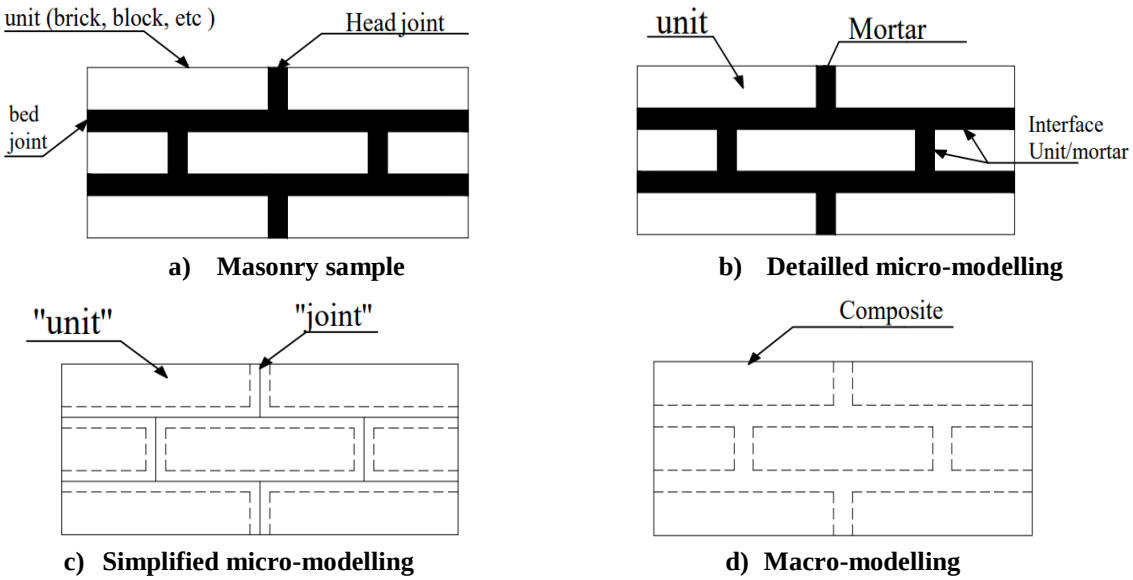

a) Masonry sample **b) Detailled micro-modelling**

c) Simplified micro-modelling **d) Macro-modelling**

Fig. 4. Material modeling techniques (Hokelekli and Yilmaz, 2019)

The mechanical material parameters for the interfaces and masonry units are determined based on relevant literature sources (Borlenghi et al., 2023; Pepi et al., 2021; Ashayeri et al., 2021; Güllü and Özel, 2020; Alpaslan et al., 2023; Gaetani et al., 2021; Gönen and Soyöz, 2022; Stockdale et al., 2019; Ferrero et al., 2021). The material characteristics for masonry and backfill are shown in Tables 1 through Table 4 (Azar and Sari, 2023, 2024, 2025).

4. Material Properties

4.1. Material Model

Concrete Damage Plasticity (CDP) presents a commendable approach for accurately representing two common types of failure, namely tensile cracking and compressive crushing. This modeling technique efficiently integrates the deterioration of materials under cyclic stress conditions.

Figure 5 illustrates the inherent behavior of masonry when subjected to both tensile and compressive loads. Within the context of tensile behavior, the material exhibits a linearly elastic response until it reaches a point known as σ_{t0}. Micro fracture is the result of a material reaching its maximum stress.

Table 1. Plasticity parameters of the CDP model

Parameter	Value
Dilation angle (ψ)	20°
Eccentricity (ε)	0.1
f_{b0}/f_{c0}	1.16
K_c	0.667
Viscosity parameter	0.01

Table 2. Basic material properties

Part	ρ (Kg/m^3)	E (Mpa)	υ
Pier	2200	3500	0.2
Cutwater	2200	2800	0.2
Arch	2200	3360	0.2
Backfill	2000	500	0.2
Spandrel wall	1900	1500	0.2
Deck	2000	1500	0.2

Note: E: isYoung's modulus; ρ: is density; υ: is poisson's coefficient.

Table 3. Input parameters for backfill material

ρ (Kg/m^3)	E (N/mm^2)	υ	c (MPa)	∅ (°)
1900	500	0.2	0.05	35

Table 4. Inelastic material parameters

Part	f_t (Mpa)	f_c (Mpa)	G_f (Mpa)
Pier	0.71	7.06	45
Arch	0.84	8.4	54
Spandrel wall	0.32	3.15	20.3

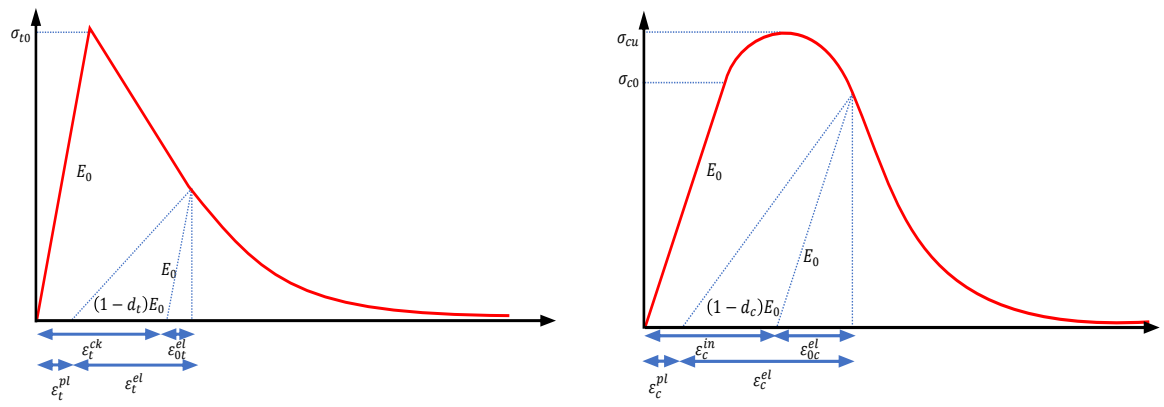

(a) **(b)**

Fig. 5. Representation of the masonry constitutive behavior in: a) Tension; and b) compression

After reaching its maximum point, the material exhibits a softening behavior in relation to the stress-strain relationship, as depicted in Figure 5a. Material undergoes deformation when it is compressed, and this deformation is observed at the point where the stress is at its maximum. At the point of maximum stress, the material demonstrates a softening behavior, as shown Figure 5b.

The CDP model may be characterized in terms of stress and strain, as follows.

$$\sigma_t = (1 - d_t) D_0^{el} : (\varepsilon - \varepsilon_t^{el}) \quad (1)$$

$$\sigma_c = (1 - d_c) D_0^{el} : (\varepsilon - \varepsilon_c^{el}) \quad (2)$$

where t: stands for tension, c: is denoted as compression, σ_t: is tensile stress and σ_c : compressive stress. ε_t^{el}: is plastic strain in tension and ε_c^{el}: is denoted as compression strain. Additionally, d_t and d_c; are variables that signify damage, and D_0^{el}: stands for undamaged initial elastic modulus.

4.2. Mohr-Coulomb Constitutive Model

The fill material commonly comprises soil, unbounded masonry, or rubble. The current study utilizes this material model to integrate the infill (Table 3). The Mohr-Coulomb criterion states that the yield point of a material is determined by the linear correlation between the shear stress acting on any point in the material and the normal stress acting on the corresponding plane (Figure 6).

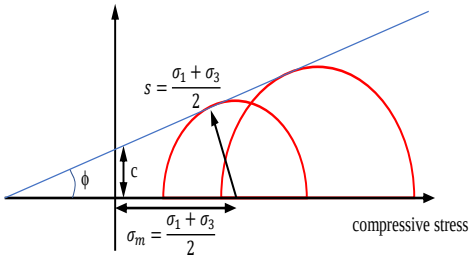

Fig. 6. Mohr–coulomb material model

In the Mohr-Coulomb material model shear stress (τ) can be characterized as a function of normal stress (σ), cohesion (c) and internal friction angle (φ) (Eq. (3)).

$$\tau = c + \sigma \tan \emptyset \quad (3)$$

The M-C model may be stated by three stress invariants, which are equivalent to pressure stress as Eq. (4).

$$p = -\frac{1}{3} trace(\sigma) \quad (4)$$

Eq. (5) represent the Mises equivalent stress.

$$q = \sqrt{\frac{3}{2}(S:S)} \quad (5)$$

where S: is stress deviator.

Eq. (6) states deviatory stress (R_{mc}) as follows.

$$R_{mc}(\theta.\varphi) = \frac{1}{\sqrt{3}\cos\varphi} \sin\left(\theta + \frac{\pi}{3}\right) + 1/3 \cos\left(\theta + \frac{\pi}{3}\right) \tan\varphi \quad (6)$$

5. Verification of FE Model

A verification study was carried out on masonry arch bridges by Fanning and Boothby (2001) to establish the appropriate material properties required for accurately simulating this specific structural type. The bridges were subjected to tests in which a reference frame was placed under the bridge, Linear Variable Differential Transformers (LVDT) were attached to measure the structural displacements and a vehicle was loaded with a specific weight.

Modeling parameters such as support conditions, properties and masonry stiffness were determined by fitting the finite element model to the test results. The behavior of masonry was replicated by utilizing a solid component modeled in terms of rigidity, incorporating features such as cracks and crushing.

The infill material was characterized using a Drucker-Prager material model, while the interface between masonry and infill was defined as a friction contact surface. The bridges were subjected to operational loads in a simulation, and the results of the model were compared with the results of on-site tests of the structures. By

considering the relevant material properties and visually inspecting the material and construction of the structure, a three-dimensional nonlinear finite element analysis program can be used to accurately predict the performance of an arch bridge.

Griffith bridge has a span of 9.49 m, a height above the abutments of 2.67 m, a width of 7.85 m and an arch ring thickness of 45 cm. The front segment of the arch ring is made of granite, while the rest of the arch ring is made of limestone, with joints around 0.5 cm thick.

The spandrel walls are made of limestone blocks with a joint thickness of around 1 cm. The examination and computational analysis of the Griffith bridge in Dublin, Ireland, are showcased in Figure 7. Figure 8 displays the finite element simulation of the deformation of the arch barrel and spandrel walls under the scenario where a fully loaded truck places its rear axle at the center of the span. Figure 9 exhibits the comparative data derived from numerical simulations and physical experiments conducted at the midpoint of the bridge's central axis during the passage of the fully loaded truck.

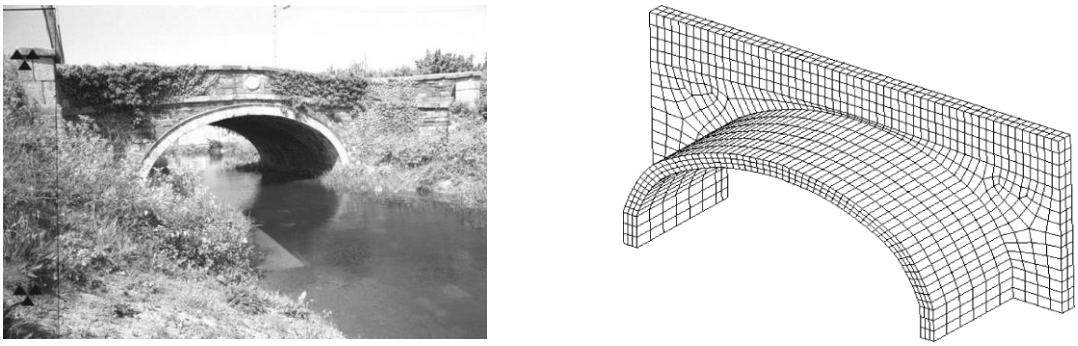

Fig. 7. Griffith bridge in Dublin, Ireland

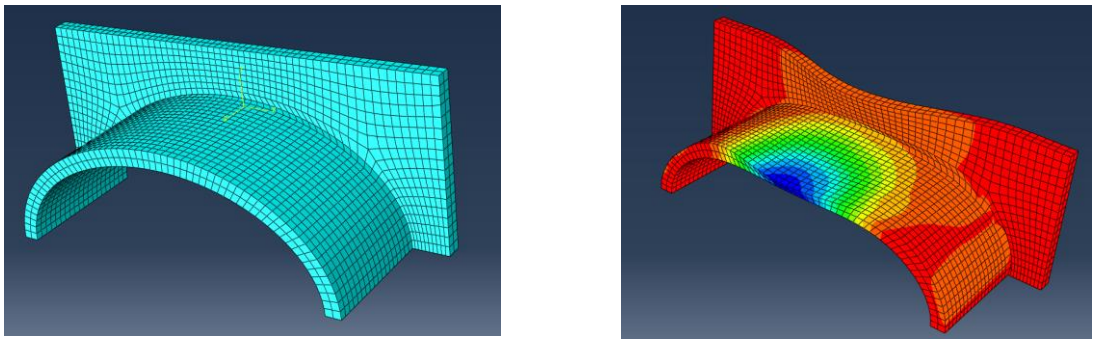

Fig. 8. Deformation of the arch barrel and spandrel walls

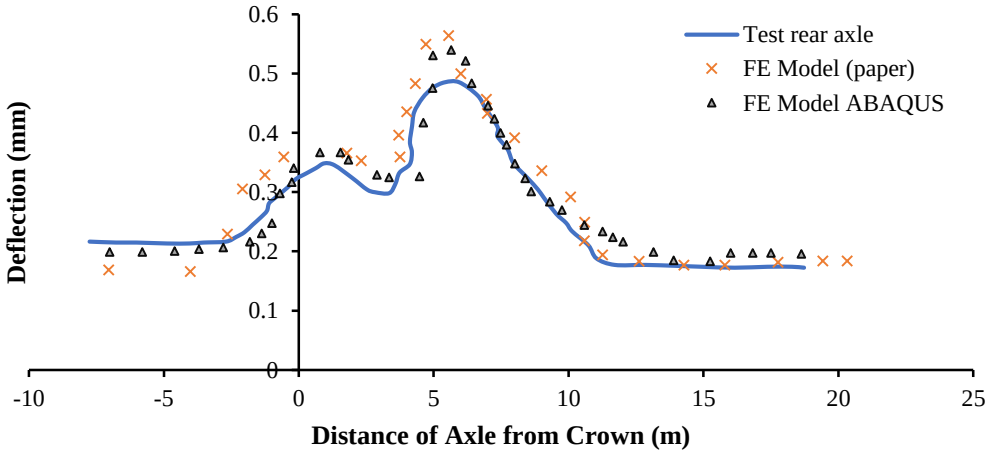

Fig. 9. Numerical and test crown displacements for fully loaded truck

The study indicated a maximum deflection of 0.43 mm in the experimental results, while the finite element model predicted a deflection of 0.54 mm.

6. Modal Analysis

The structural behavior of masonry bridges is influenced by various characteristics that have been shown to have significant effects. Factors such as the overall length, the number of spans, the maximum length, the height, the arch type and the material properties are essential in this context. The accurate assessment of structural performance requires the application of finite element modelling. The validation of the initial finite element model in masonry structures requires the use of tests or empirical equations. In a study by Bayraktar et al. (2022) statistical methods were used to establish a quantitative correlation between the maximum arch span and the initial natural frequencies of eight masonry bridges. This correlation was determined by analyzing the respective natural frequencies by using Eq. ().

$$y = -3.935 \ln(x) + 16.824 \quad (7)$$

where x and y: denote the maximum arch span (measured in meters) and the first frequency (expressed in Hertz), respectively. Table 5 displays the theoretical frequency values calculated using Eq. (7) and the experimentally determined first frequency values. The results indicate a strong agreement between the experimentally observed and theoretically predicted values.

Consequently, it is proposed that Eq. (7) is suitable for validating the analytical model of masonry bridges. Given the minimal discrepancy between the experimentally obtained and theoretically calculated initial frequency values, the authors suggest that the finite element model constructed accurately reflects the real structural response. The mass contribution ratio and the analysis of the mode motions show that the first and third as well as the fifth mode shape significantly influence the behavior of the model.

Table 5. Correlation between the dynamic characteristics of the bridges

Bridge type	Span number	Length of span	The first natural frequency (Hz)	
			Experimental	Empirical, Eq. ()
Stone Masonry	Seven	16	5.890	5.914
Stone Masonry	Single	16	5.279	6.123
Stone Masonry	Single	19.5	6.063	5.137
Stone Masonry	Two	25	4.640	4.126
Stone Masonry	Single	25	4.045	4.189
Stone Masonry	Eight	15	4.730	6.168
Stone Masonry	Two	10	8.853	7.763
Stone Masonry	Two	12	6.970	7.046

Table 6. Numerical natural frequencies and ratios of the effective mass to the total mass in the three main directions

Mode	f (Hz)	$m_{eff,x}/m_{tot}$ (%)	$m_{eff,y}/m_{tot}$ (%)	$m_{eff,z}/m_{tot}$ (%)
1	8.8076	0	0	24.02
2	9.3167	0	0	0.1
3	9.8325	0.1	0	12.7
4	10.470	0.4	0	0
5	11.010	35.4	0	0
6	11.196	0.1	0	6.55
7	12.067	0	0	0.4
8	12.943	0	0	0.2
9	13.092	0	0	4.60
10	14.078	0	0	0.1

Table 6 shows the distribution of the initial 10 modes of the Halilviran bridge in both longitudinal and transverse directions. In addition, the deformed shapes of the primary modes are shown together with their respective periods and the mass ratio involved (PMR) in the main directions. The first mode (with a period of 0.11 s) involves the deck, with the transverse direction having a PMR value of 24.02%.

The third mode, with a period of 0.10 s, affects the upper part of the piers and the parapet walls. The PMR in the transverse direction is 12.72%. The fifth mode with a period of 0.09 s (T = 0.09 s) concerns the filling and the deck of the bridge. It has the highest PMR of 35.4% in the longitudinal direction. The sixth vibration mode with a period of 0.08 s concerns the parapet wall of the bridge. It has the highest PMR of approx. 6.55% in the transverse direction.

7. Nonlinear Analyses

In the subsequent phase, the model is subjected to two horizontal components of ground motion for dynamic analysis. The full Newton-Raphson method is used to solve the nonlinear equilibrium equations by a stepwise integration approach with a time step of 0.005 s. Rayleigh damping refers to the dissipation of energy resulting from phenomena that are not explicitly accounted for in the constitutive law of the material. The viscous damping coefficients for masonry are typically between 2% and 10%.

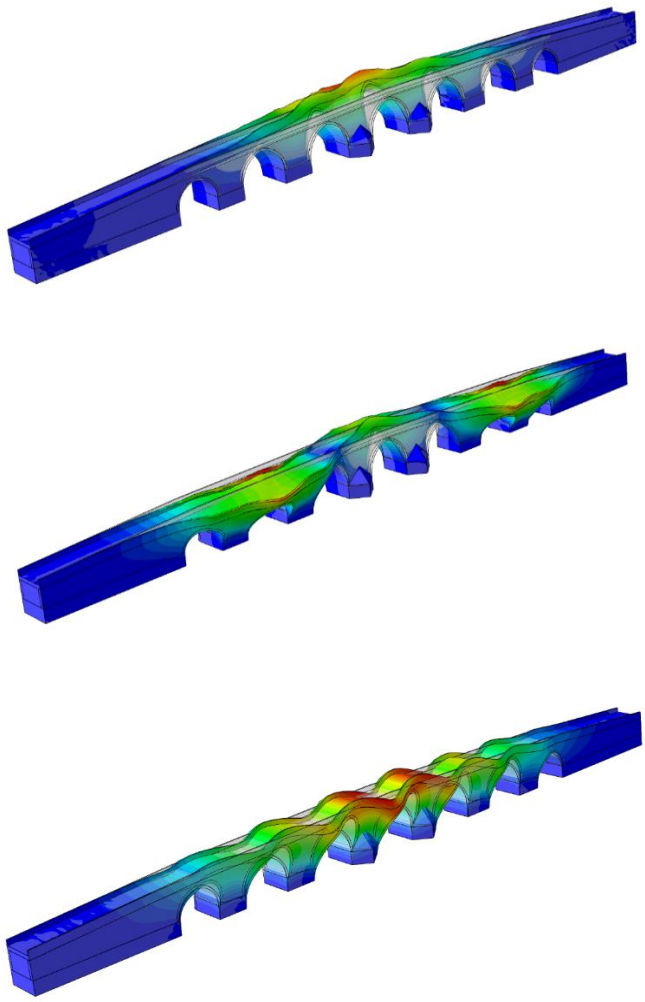

Fig. 10. Distribution of the modes in the longitudinal and transversal directions. Deformed shapes of the first main modes, corresponding periods and participating mass ratios

In this research, the model is exposed to a damping ratio of 3%, which is established through an analysis of the first frequency and the frequency at which the modal mass contribution ratio surpasses 90%. This study uses acceleration data that was recorded during the Düzce earthquake sequence on August 17, 1999. Figure 11 depicts the time history of acceleration, specifically the two horizontal components, with respect to the Peak Ground Acceleration (PGA) of 0.36 g in the longitudinal and transverse directions. The decision was made to restrict the duration of the accelerograms to 5 s (between the 7th and 12th second of the graph) in order to manage the substantial computational resources needed for the analyses.

8. Results

An evaluation of the overall performance of the masonry bridge is carried out through a comparative analysis of results. Initially, this comparison involves an assessment of the amount of energy absorbed by the model. The energy equilibrium of the system under seismic activity can be elucidated by Eq. (8). Within this equation, various variables are defined; (EI) the energy input from the earthquake $(W\xi)$, represents the energy dissipated as a result of viscous effects (Wp), accounts for the hysteretic energy encompassing plasticity and damage (We), signifies the elastic-strain energy and (Wk), stands for the kinetic energy.

$$EI = W\xi + Wp + We + Wk \quad (8)$$

The overall elastic vibrational energy, represented as Wev, is the combination of the elastic strain energy (We) and the kinetic energy (Wk). Eq. (8) can be reformulated in a different manner.

$$EI - Wev = W\xi + Wp \quad (9)$$

The cumulative energy absorption in Eq. (9) is delineated on the right-hand side. Specifically, $W\xi$ comprises the dissipated energy from viscous effects, which includes the dissipation of soil through dashpots denoted by $W(\xi.s)$ and $W(\xi.r)$ the portion attributed to the structure through Rayleigh damping.

Conversely Wp represents the energy dissipation by the structure through plasticity and damage. The computation of $W(\xi.s)$ involves the integration of dashpot coefficients and the square of velocities across the dashpots over time. To ensure reproducibility of results, the variable EI, signifies the external work in the analysis.

Additionally, $W\xi$ denotes the energy dissipated due to viscous effects, while Wp, represents the combined energy dissipated by plastic deformation and damage. The variable We, signifies the recoverable strain energy, and Wk represents the kinetic energy. In the base-fixed model, $W\xi$ and $W(\xi.r)$, coincide due to the absence of dashpots.

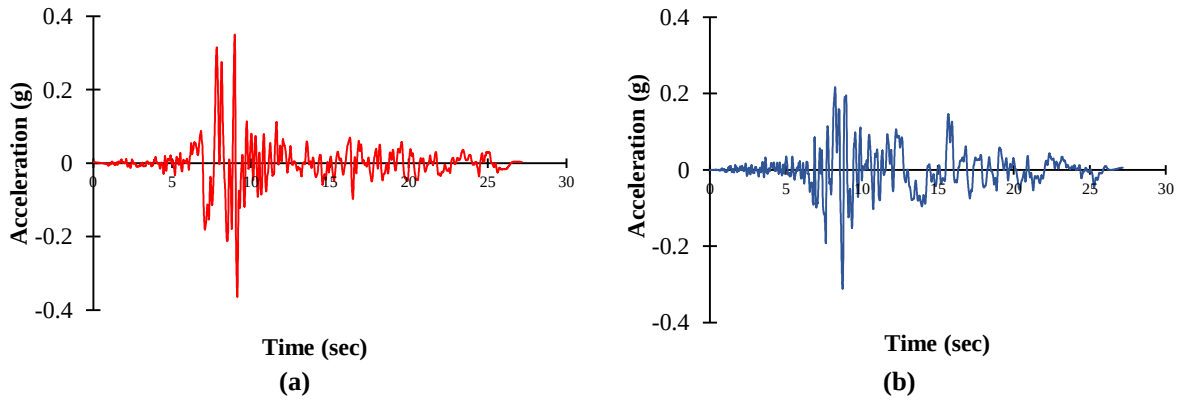

Fig. 11. Horizontal components of the real accelerograms used in the non-linear dynamic analyses: a) Longitudinal direction; and b) Transversal direction

Figure 12 illustrates the variations over time in the energies (EI). (Wξ). (Wp). (We) and (Wk). within the model. The primary dissipation of input energy occurs due to plastic deformation. This phenomenon is attributed to the localized damage in a limited number of elements, thus validating the suitability of the selected CDP parameters. The study investigates the impact of tension and compression-induced damages on masonry materials, particularly in the context of seismic damage assessment for masonry bridges. Tensile cracks and compressive crushing are the two main forms of damage observed in masonry materials, with tension being a significant factor due to the lower tensile strength compared to compressive strength. The research focuses on analyzing the effects of tension and pressure-induced damages on masonry bridges during seismic events. Tensile fractures in bridges occur when the predicted plastic strains and main stresses in tension surpass specified threshold values.

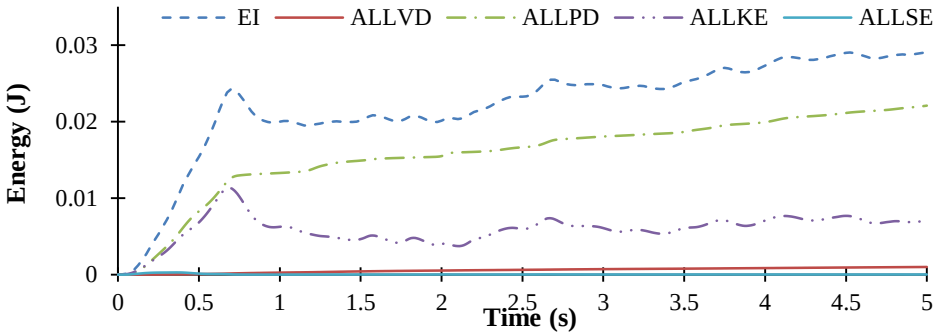

Fig. 12. Total input energy (EI), energy dissipated by viscous effects (Wξ), hysteretic energy (Wp), kinetic energy (Wk) and elastic-strain energy (We)

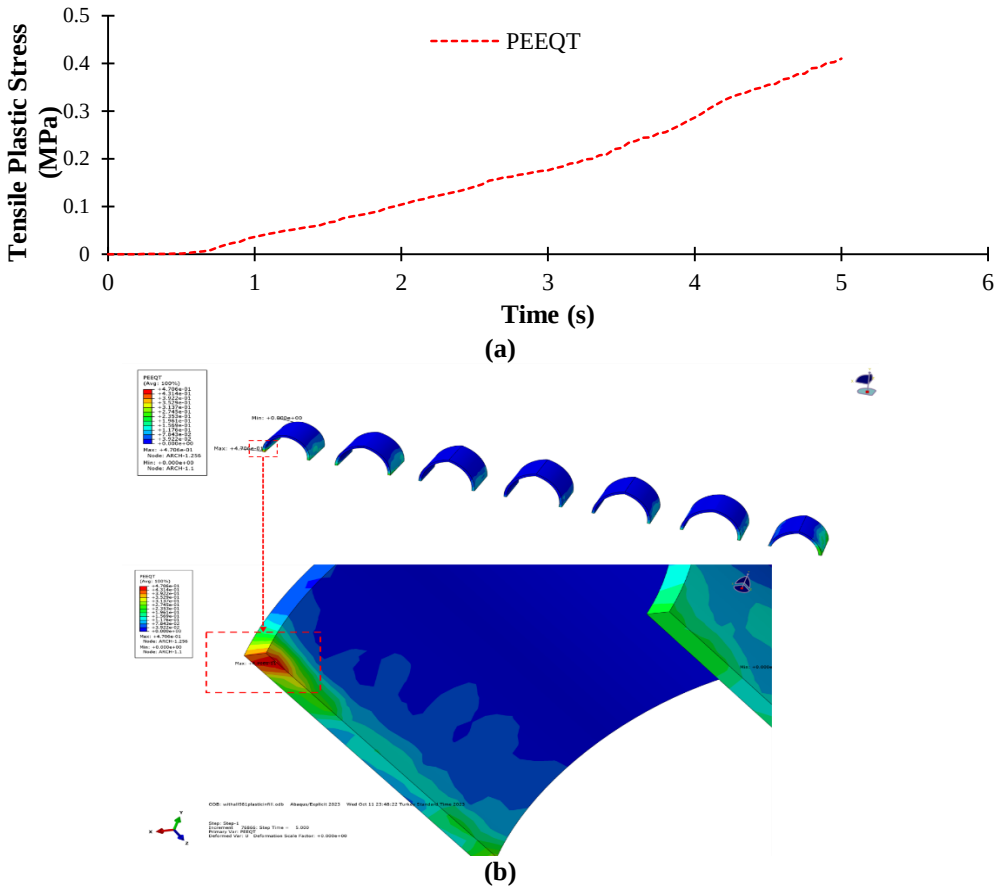

Fig. 13. a) Time histories; and b) Maximum principal (tension) strain contour maps of the arch

The study utilizes Figures 13 and 14 to present the maximum values and patterns of equivalent plastic tensile strains (PEEQT) in masonry arches and spandrel walls under the influence of longitudinal and transverse strong ground motions. The distribution of equivalent plastic tensile strain (PEEQT) after 5 s of earthquake records reveals concentrated tensile plastic deformations around the bearing portion connecting the arches of the wall.

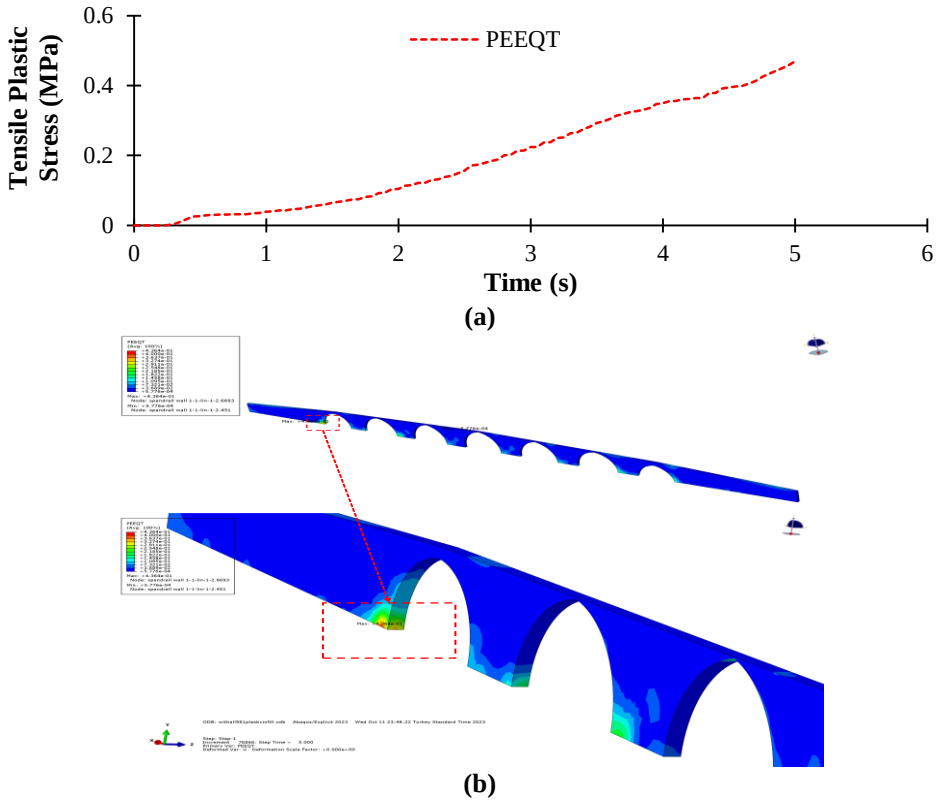

Fig. 14. a) Time histories of the spandrel wall; and b) Maximum principal (tension) strain contour maps

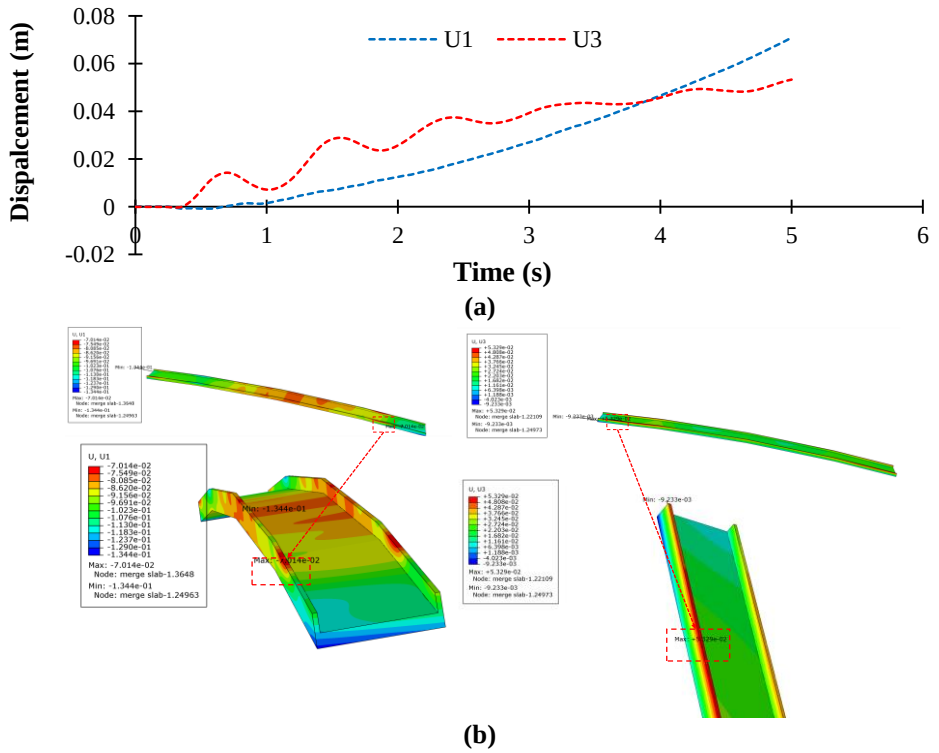

Fig. 15. A) Transverse displacement; and b) Longitudinal of the bridge deck

The masonry arches and spandrel walls exhibit peak plastic tensile strains of $4.7e^{-1}$ and $4.36e^{-1}$, respectively, with the strains predominantly localized in the lower interior sections of both structures. Additionally, the study highlights the maximum displacements of the bridge deck in the longitudinal and transverse directions, as depicted in Figure 15. Figure 16 illustrates the dynamic displacements graphed in the horizontal directions at the upper and lower ends of the spandrel walls of the bridge. This graph illustrates the significance of the structural response in masonry bridges that takes place out of the plane.

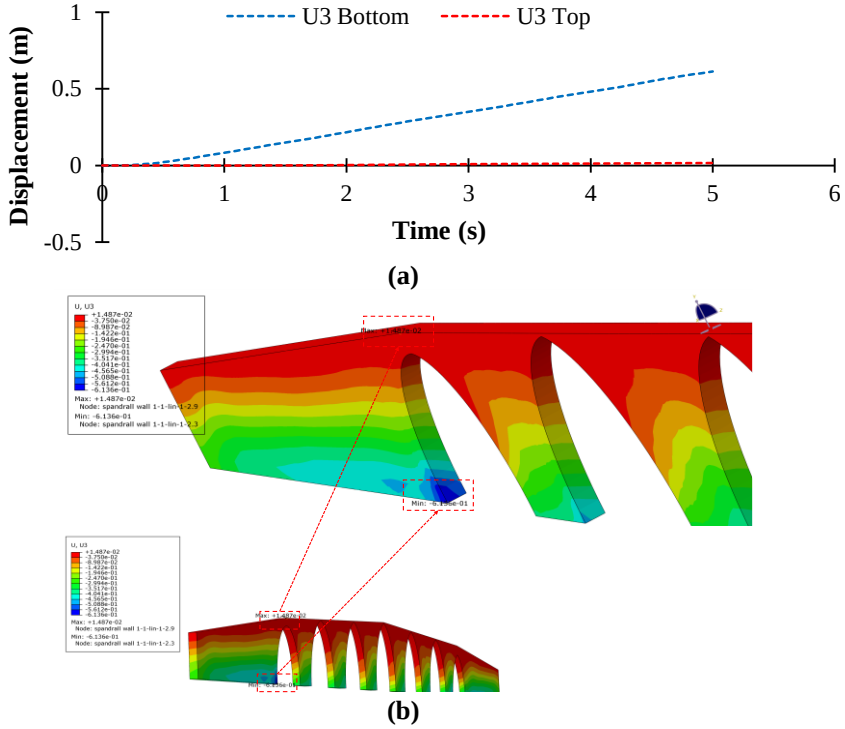

Fig. 16. a) Time histories of the spandrel wall; and b) Displacements in the transverse directions at the bottom contour maps

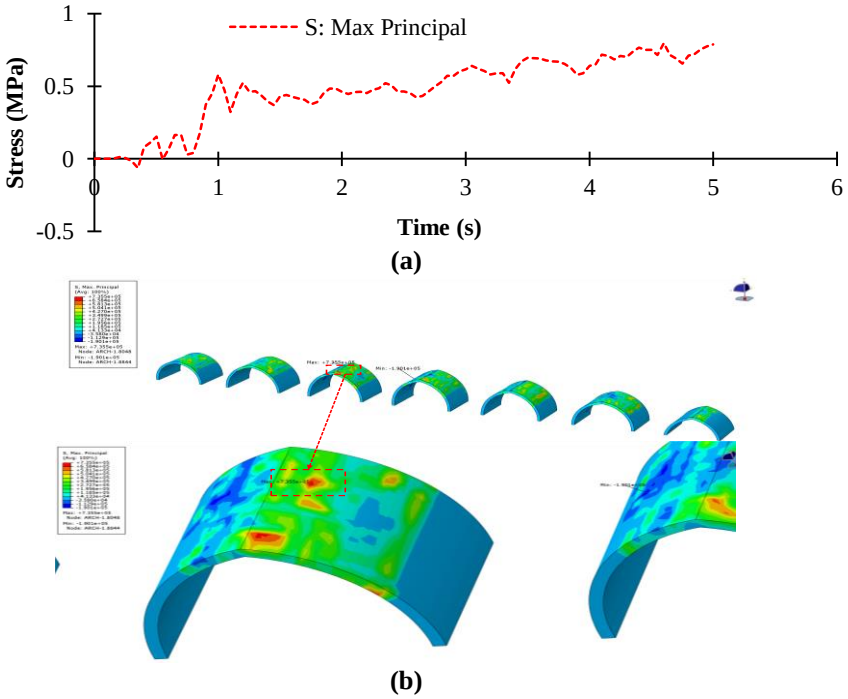

Fig. 17. a) Time histories; and b) Maximum principal (tension) stress contour maps of the arches

The measurements are carried out to determine the horizontal displacements of the spandrel wall, leading to the manifestation of out of plane characteristics in the wall. The longitudinal displacements of the spandrel wall are assessed to establish its in-plane behavior. The stability of the spandrel walls and their relationship with the arch barrel are crucial elements influencing the various challenges observed in masonry arch bridges. Figures 17-19 illustrate that the masonry unit undergoes peak principal stresses when exposed to intense ground motion along the arch interface.

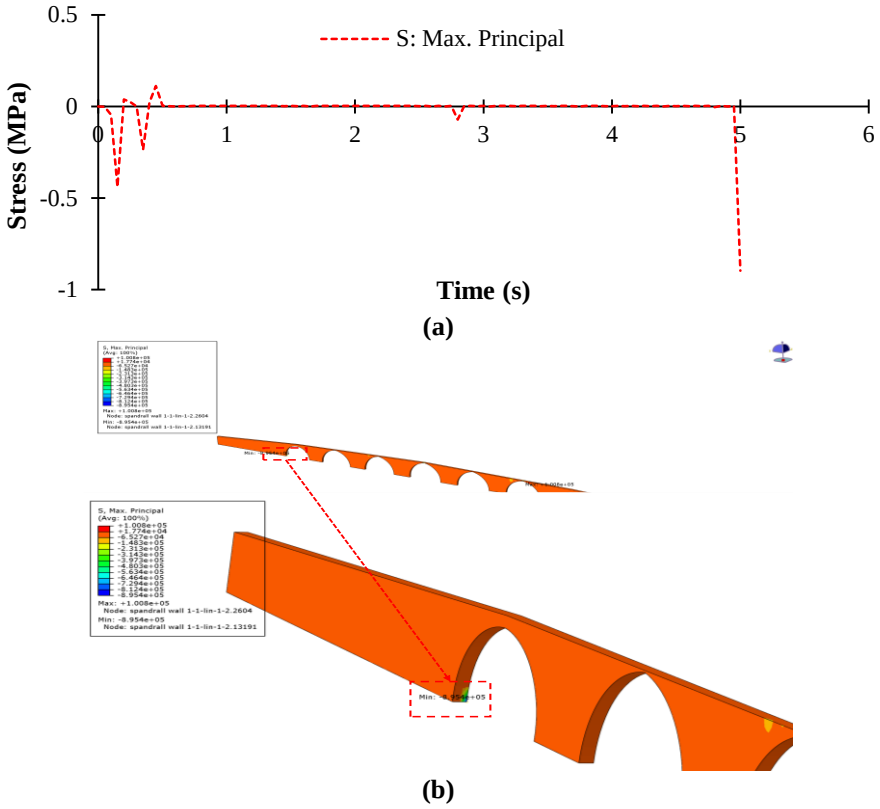

Fig. 18. a) Time histories; and b) Maximum principal (compression) stress contour maps of the spandrel wall

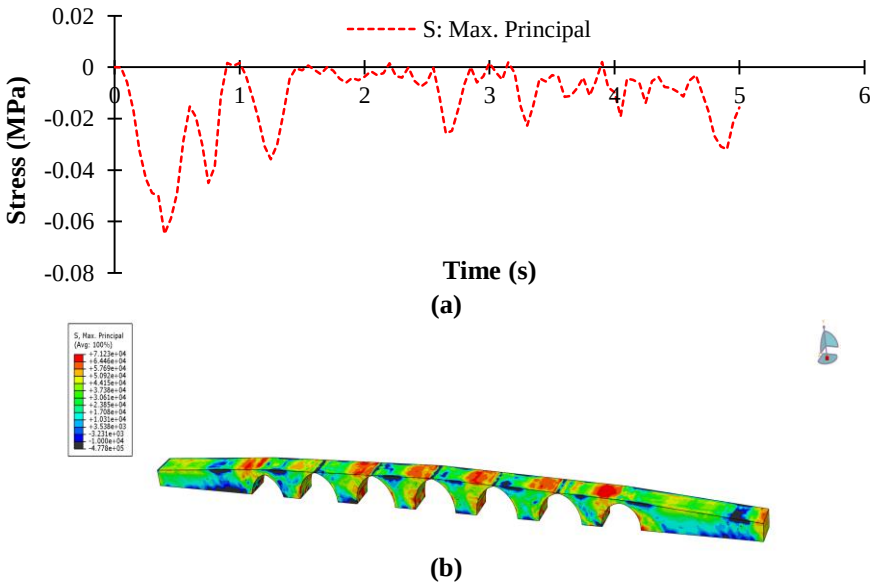

Fig. 19. a) Time histories; and b) Maximum principal (compression) stress contour maps of the infill

Figures 20 and 21 illustrate the changes over time in the minimum principal stresses and the specific stress regions. The minimum principal stresses determined in the analysis were below 3.15 MPa, which is the upper limit for compressive stresses in masonry walls and vaults. However, the model showed increased stresses in certain segments of the bridge that approached the maximum allowable value.

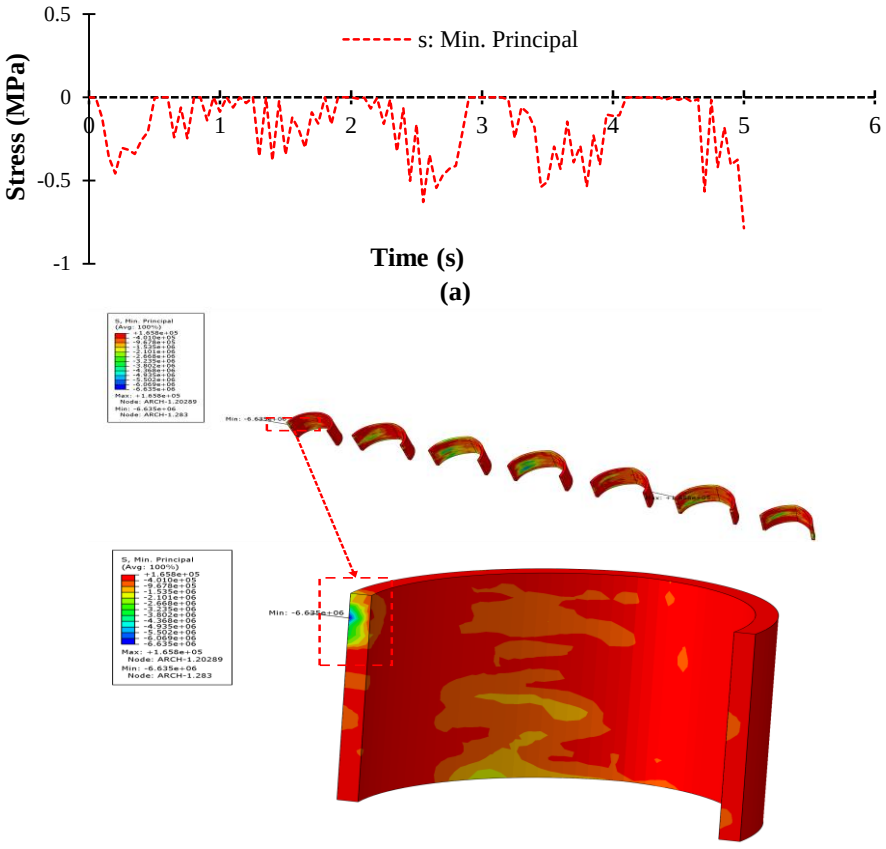

Fig. 20. a) Time histories; and b) Minimum principal (compression) stress contour maps of the arches

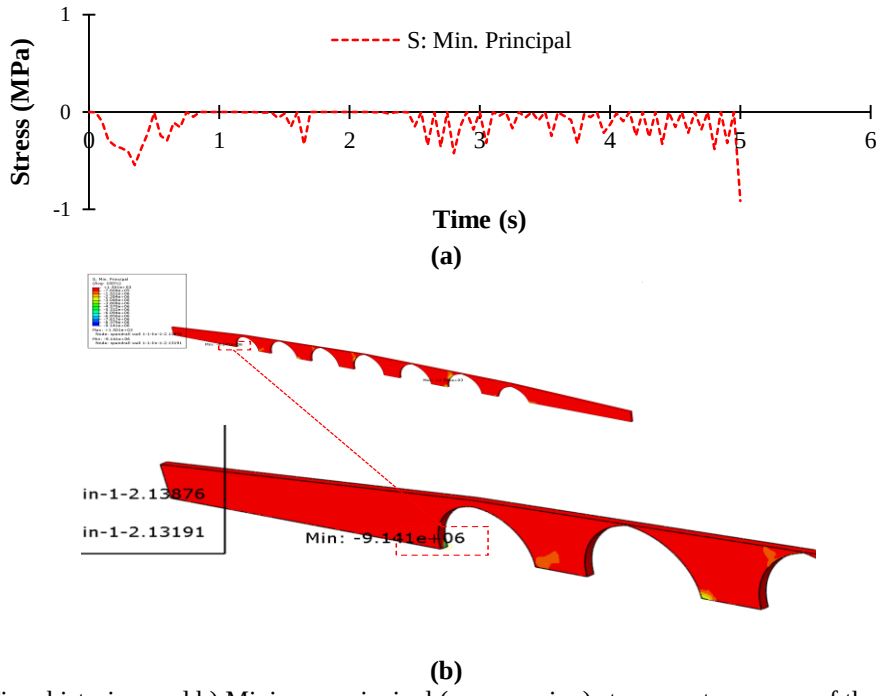

Fig. 21. a) Time histories; and b) Minimum principal (compression) stress contour maps of the spandrel wall

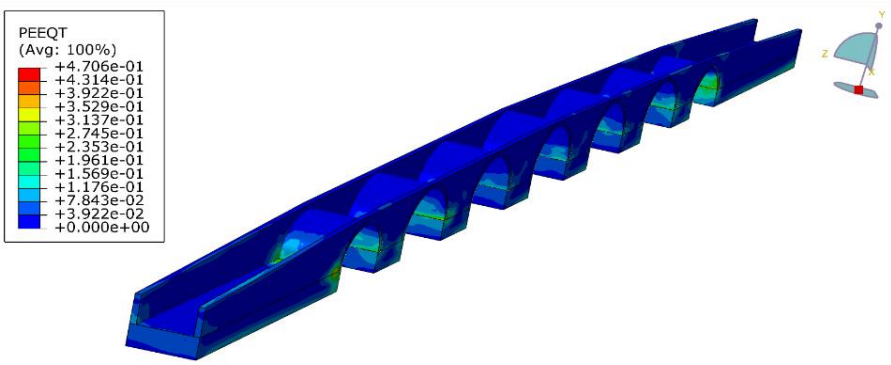

Fig. 22. Maximum principal (tension) strain contour maps of the bridge

9. Post-Earthquake Survey

In this section the findings of the prompt evaluation conducted after an earthquake on a total of five bridges situated within or near the city of Glina. A visual inspection was conducted by Perković et al. (2021), Novak et al. (2020), Miranda et al. (2021), Korbar et al. (2021), and Cassese et al. (2020) for the assessment, using a pre-established process.

Two significant earthquakes struck North-western Croatia. The earthquake occurred in March 2020 and the second one took place in December 2020. After Petrinja earthquake for bridges in and around the town of Glina started.

9.1. Matija Gubec Street Bridge

The cross-sectional design of the bridge consists of three steel elements, along with an 18 cm thick concrete surface. The superstructure has a width of 4 m. The seismic activity had a noticeable effect on the stone wall connections, resulting in cracks and openings of various centimeters.

The absence of mortar and displacement of the stone blocks were observed. The abutment exhibited indications of both lateral shifting and rotational motion towards the bridge opening due to ground movements. Evidence of soil erosion was observed at the abutment wings.

9.2. Roviška Bridge

The bridge is built with reinforced concrete and comprises more than three spans. The superstructure is composed of a reinforced concrete slab directly supported by substantial columns projecting outward at the upper end. The asphalt connection linking the abutment and superstructure sustained no damage, and there were no discernible movements at the superstructure supports. The columns and abutments showed no notable indications of cracks, rotations, or settlements. Subsequent to the earthquake, the bridge continued to operate as intended.

9.3. Svracica Bridge

The superstructure of the bridge consists of two continuous composite girders spanning four evenly distributed sections. It is constructed with a composite cross-section comprising multiple steel girders. Despite the earthquake, no significant damage, such as permanent deformations or displacements, was observed in the superstructure or substructure components. Consequently, regular maintenance was conducted to ensure the bridge's unrestricted operation. However, further examination and upkeep are advised due to the deterioration of the steel girders and indications of corrosion in the column reinforcement.

9.4. Nikola Tesla Street Bridge

The bridge is a truss structure with three continuous girders spanning across. The superstructure of the construction is composed of steel girders and concrete ribs, which are filled with concrete and positioned between two sets of steel girders.

The steel girders are partially embedded

within these ribs, serving as a formwork for the concrete. The bridge did not exhibit significant structural damage as a result of the earthquake, neither in the upper structure, lower structure, nor the inclined surfaces surrounding the supports.

Fractures were observed in the region where the superstructure connects to the abutment, specifically at the point where the abutment wall intersects with the cross girder and provides support for the superstructure.

9.5. Hader Bridge

The bridge consists of a continuous slab girder with multiple spans and a simply supported girder that extends across. The structure sustained damage from an earthquake on various structural elements.

The movement of the bridge superstructure in both the longitudinal and transverse directions was clearly noticeable at a significant pace. Extensive review of literature and in-depth analysis of design experience consistently indicate that columns are widely recognized as the most critical element in the seismic evaluation of reinforced concrete road bridges. The main factors contributing to structural defects in columns include inadequate dispersion of longitudinal and transverse reinforcement, poor concrete quality, insufficient seismic design, concrete degradation, reinforcement and steel girder corrosion, railing and bearing deterioration, obstruction of expansion joints, asphalt cracking, and erosion of abutment slopes (Kassem et al., 2022). The ability of columns to deform is essential in dissipating seismic energy.

Assessing the ductility of older bridges that do not meet current seismic design standards is a challenging task. Earthquakes often lead to shear critical brittle fracture in columns due to the limited shear capacity of short piers, while tall pillars may collapse due to flexural failure. To extend the applicability of the findings to other ancient masonry multi-span arch bridges, it is important to consider the influence of differential settlements on their structural capacity. Accurate estimation can only be achieved through the use of a sophisticated model that accounts for the interaction between soil and structure, known as Soil-Structure Interaction (SSI).

Several bridges have been recognized as significant structures requiring maintenance through proper restoration methods and suitable construction materials (Samadi et al., 2021). Therefore, understanding the composition of construction materials, different structural components, and their overall structural integrity is essential. To fully comprehend the structural behavior of masonry arch bridges, it is crucial to have knowledge about the fundamental structural elements that constitute them. Understanding the performance of masonry bridges and their ability to withstand changes in structural components requires an appreciation of their load-carrying capacities and an evaluation of the structural integrity and intensity of the load they support.

10. Conclusions

This study showed that it is possible to perform a seismic assessment with a simplified method using a limited data set, even in a complex environment with different modelling factors. A detailed three-dimensional FE model was created to investigate the dynamic properties of the bridge. This model effectively represented the complex geometric details obtained from laser scanning and photogrammetric surveys. The material properties of the bridge components were evaluated by diagnostic and geognostic investigations and by consulting the relevant literature. By using acceleration diagrams consisting of two horizontal diagrams showing the longitudinal and transverse alignment of the bridge, the study provided the following results:

- This research showed that the point cloud generated by terrestrial laser scanning technology provides fast and highly accurate data to determine the essential

structural geometry required for structural analysis. The point cloud data was used to create a computerized solid element model of the building. Once the modeling process was completed, load and material assumptions were determined and then static and dynamic evaluations of the structure were performed.

- Bridge failure primarily happened at the junction between the parapet walls and the barrels, as well as with the masonry arch, which are the most susceptible elements of the bridge (see Figure 22).
- The bridge exhibited dynamic properties, as the first analysis of its natural frequency showed. Furthermore, the results of the non-linear dynamic simulations underlined the vulnerability of the bridge to seismic forces and indicated a significant vulnerability. A comprehensive understanding of the behavior of the various macro elements that make up the bridge was achieved by comparing contour plots showing tensile damage, displacements and dissipated energy.
- The preliminary results of the natural frequency analysis provided valuable insights into the dynamic properties of the bridge. The Halilviran bridge exhibited three predominant modes, each characterized by a significant PMR. The presence of masonry affected the fundamental behaviors of the bridge and thus influenced its overall structural integrity. The primary vibration patterns of the bridge had a short duration, leading to a significant increase in spectral accelerations and subsequent remarkable structural deterioration.
- In model, the 1st and 3rd mode shapes occurred in the transverse direction, whereas the 4th and 5th mode shape occurred in the longitudinal direction (Figure 10).
- Figure 12 showed the overall energy dissipation of the bridge as part of a non-linear dynamic analysis. Most of the energy introduced into the system was dissipated by structural plasticity mechanisms. In accordance with the existing literature, the generalization of these results should be taken with caution, as the response of a bridge structure to seismic events depends on various factors, including the dynamic properties of the system, the choice of foundation model, soil type, and frequency spectrum of seismic waves.
- Examination of the contour plots of the plastic strain damage showed that the bridge shows signs of degradation, particularly in the parapet wall, the upper sections of the arches and the infill. The choice of infill material played a crucial role in improving the structural stability of bridges, especially when considering the specific reinforcement method used. This strategy has the potential to improve the reinforcement of masonry bridges.
- Prior studies in the literature, specifically by Seker et al. (2014) have recommended the utilization of the subsequent equation to determine the maximum relative displacement requirement for masonry structures. Consequently, this investigation also incorporates Eq. (10) for the evaluation of displacement values.

$$\Delta_{imax} \leq \frac{0.02 * h_i}{R} \tag{10}$$

wher h_i and R: denote the height of the structure and the behavior factor related to the ductility of the structure, respectively. Low bridge $h_i = 9$ m, $R = 2$ and the corresponding maximum allowable top displacement is 0.09 m. The study revealed that the displacements observed at the interlock points between the arches and spandrel wall with the piers are greater in analyses compared to the values computed using the provided formula. Consequently, it can be inferred that the displacements exceed the permissible thresholds.

- The inclusion of fill material in a masonry arch bridge provides several beneficial effects that enhance its load-bearing capacity. Firstly, the additional weight of the infill material applies

compressive stresses on the arch, thereby improving its stability. Additionally, it assists in distributing dynamic loads from the roadway to the upper section of the arch.

Moreover, it prevents horizontal movements of the arch by utilizing passive ground pressures. Nonetheless, the study indicated that improving the mechanical properties of the backfill could significantly enhance the seismic response of the bridge (Martinelli et al., 2018). This is particularly evident in the cases of elastic modulus and increases in cohesion.

- The investigation revealed that the primary stresses caused by both out of plane and in-plane seismic forces exceeded the critical tensile stress threshold of 0.32 MPa for masonry walls. The potential collapse of the bridge could be significantly affected by the out-of-plane behavior of these elements under lateral seismic forces. Specific retrofitting measures would be essential to ensure consistent structural performance. In addition, the parapet walls are highly susceptible to seismic and train traffic loads, especially with regard to their out of plane behavior. It is therefore crucial to prioritize the repair and reinforcement of dilapidated parapet walls exposed to these loads. The most severely damaged coatings of the Halilviran bridge are obviously those exposed to significant transverse displacements or located near sections exposed to significant horizontal displacements. Figure 19 illustrated the vertical displacement of the parapet wall of the Halilviran bridge perpendicular to the bridge plane. To prevent failure in the vertical plane of the parapet walls, the tensile areas can be reinforced using various techniques. The specific configuration of the strengthening system depends on factors such as the classification of the building, cultural significance and mechanical requirements. Several techniques have been commonly proposed to improve the structural integrity of parapet walls.
- Various techniques can be employed to address issues with spandrel walls, such as using transverse tie bars, substituting backfill with concrete, reconstructing with a tapered section, grouting if needed, applying a thin concrete cover, and utilizing a Fabric-Reinforced Cementitious Matrix (FRCM) composite (Figure 23). Mokrini et al. (2012) extensively studied these methods. In cases where a spandrel wall with a tapered section is considered beyond repair, an alternative approach involves demolishing the existing walls and reconstructing them with a tapered section instead of a straight one. Additionally, adding a layer of reinforced concrete to an existing one can protect the arch and inner surfaces by applying a thin coating of reinforced concrete. Concrete filling can also be used to replace part or all of the backfill material. Transverse tie bars, known as rots, stitching, or anchoring, can be used to connect and restrain the lateral movement of spandrel walls.
- The macro modeling technique was employed to calculate the collapse loads and potential hinge mechanisms of multi-span masonry arch bridges when the micro modeling technique is deemed too intricate.

This approach is advantageous for determining the highest tensile stresses that exceed the tensile strength and identifying potential hinge mechanisms in multi-span brick arch bridges.

- The analysis of the findings indicated that the structural response and damage levels of the various macro-elements in the case study wre influenced by both their geometric characteristics and potential interactions with neighboring components.
- The absence of bending moment in arches is a widely acknowledged phenomenon, attributed to their inherent curvature properties. However, due to the interaction with other components and the inherent lack of symmetry in the load, the presence of a bending moment is inevitable.

Complex arch constructions experience both bending moments and horizontal thrusts, resulting in tensile strains being applied to the cross sections of the arch construction.

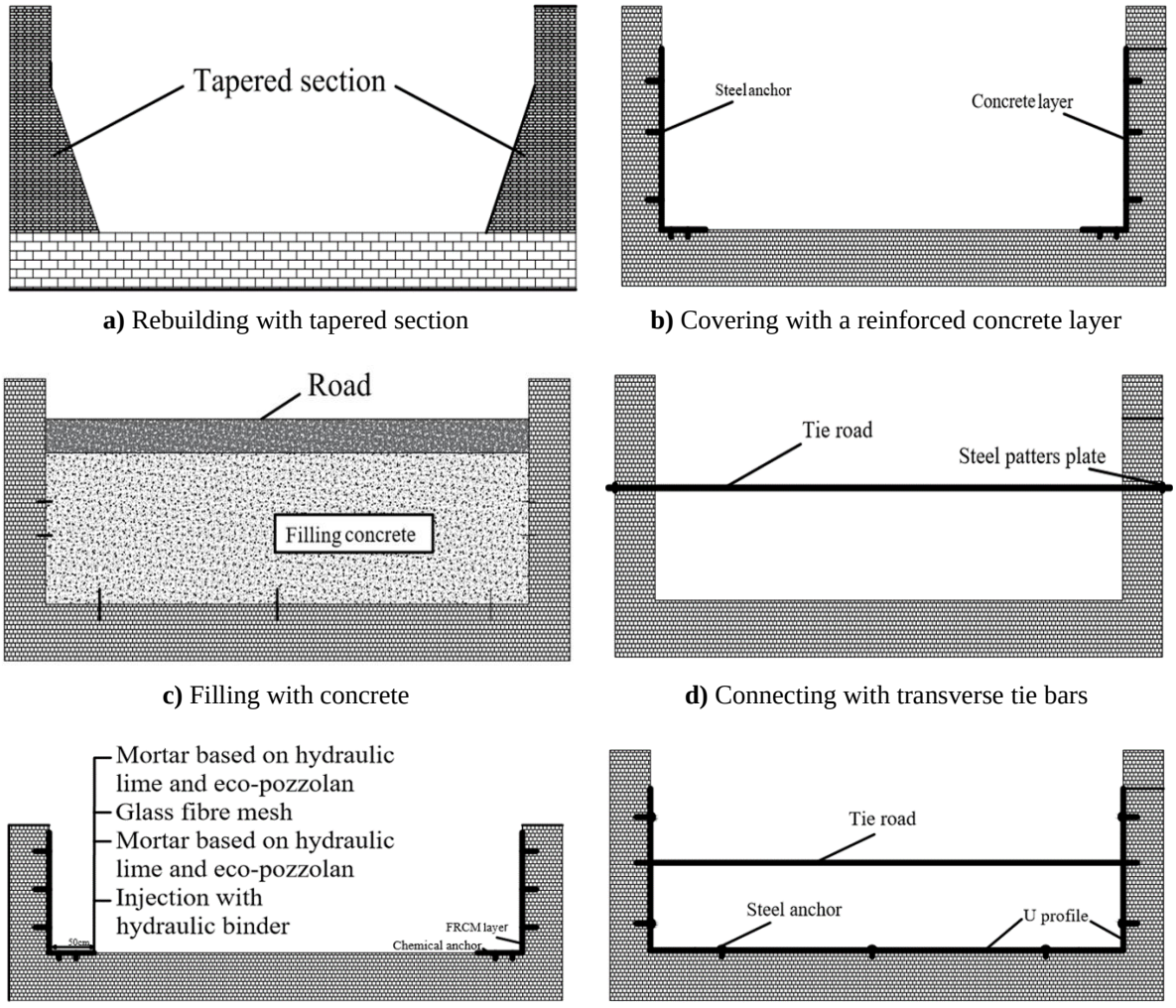

a) Rebuilding with tapered section

b) Covering with a reinforced concrete layer

c) Filling with concrete

d) Connecting with transverse tie bars

e) Covering with FRCM

f) Connecting with stainless steel U profiles

Fig. 23. Strengthening techniques for spandrel walls of masonry bridges (Bayraktar and Hökelekli, 2021)

Increasing the dead loads leads to a reduction in tensile stresses, often necessitating the use of larger cross-section dimensions for arches. This is particularly evident in old masonry structures, where engineers recognize the significant influence of the self-weight in maintaining the stability of arches. Therefore, it is crucial to consider the potential failures that may arise from geometric modifications due to retrofitting, as these adjustments can have detrimental and lasting effects on the structure.

11. Acknowledgment

The authors gratefully acknowledge the support of the YAP Project (Project ID: 43950, Project Code: MGA-2023-43950) in conducting this research.

12. References

Alpaslan, E., Yilmaz, M.F. and Sengönül, B.D. (2023). "Rating and reliability assessment of a historical masonry arch bridge", *Journal of Civil Structural Health Monitoring*,13(4-5), 1-19, https://doi.org/10.1007/s13349-023-00692-7.

Ashayeri, I., Biglari, M., Formisano, A. and D'Amato, M. (2021). "Ambient vibration testing and empirical relation for natural period of historical mosques, Case study of eight mosques in Kermanshah, Iran", *Construction and Building Materials*, 289, 123191, https://doi.org/10.1016/j.conbuildmat.2021.123191.

Azar, A.B. and Sari, A. (2025). "Reinforcement of arch structures under blast loads: A sustainable approach to structural enhancement", *Journal of Structural Integrity and Maintenance*, 10(1), 2457913, https://doi.org/10.1080/24705314.2025.2457913.

Azar, A.B. and Sari, A. (2024). "Damage identification of masonry arch bridge under

blast loading using smoothed particle hydrodynamics (SPH) method", *Structural Engineering and Mechanics*, 91(1), 103, https://doi.org/10.12989/sem.2024.91.1.000.

Azar, A.B. and Sari, A. (2023). "Historical arch bridges-deterioration and restoration techniques", *Civil Engineering Journal*, 9(7), https://doi.org/10.28991/CEJ-2023-09-07-010.

Bayraktar, A., Çalik, I. and Türker, T. (2022). "A simplified fundamental frequency formulation based on in-situ tests for masonry stone minarets", *Experimental Techniques*, 46(2), 225-238, http://doi.org/10.1007/s40799-021-00474-0.

Bayraktar, A. and Hökelekli, E. (2021). "Seismic performances of different spandrel wall strengthening techniques in masonry arch bridges", *International Journal of Architectural Heritage*, 15(11), 1722-1740, https://doi.org/10.1080/15583058.2020.1719234.

Borlenghi, P., Saisi, A. and Gentile, C. (2023). "ND testing and establishing models of a multi-span masonry arch bridge", *Journal of Civil Structural Health Monitoring*, 1-17, https://re.public.polimi.it/handle/11311/1227342.

Cassese, P., De Risi, M. T. and Verderame, G.M. (2020). "Seismic assessment of existing hollow circular reinforced concrete bridge piers", *Journal of Earthquake Engineering*, 24(10), 1566-1601, http://doi.org/10.1080/13632469.2018.1471430.

Castellazzi, G., D'Altri, A.M., de Miranda, S. and Ubertini, F. (2017). "An innovative numerical modelling strategy for the structural analysis of historical monumental buildings", *Engineering Structures*, 132, 229-248, https://doi.org/10.1016/j.engstruct.2016.11.032.

Chalajour, S. and Hataf, N. (2023). "The comparison of tunnel convergence from numerical analysis with monitoring data based on different constitutive models in rock medium", *Civil Engineering Infrastructures Journal* 56(2), 301-319, https://doi.org/10.22059/CEIJ.2022.343391.1843

Clementi, F., Pierdicca, A., Formisano, A., Catinari, F. and Lenci, S. (2017). "Numerical model upgrading of a historical masonry building damaged during the 2016 Italian earthquakes: The case study of the Podestà palace in Montelupone (Italy)", *Journal of Civil Structural Health Monitoring*, 7, 703-717, https://link.springer.com/article/10.1007/s13349-017-0253-4.

Fanning, P.J. and Boothby, T.E. (2001). "Three-dimensional modelling and full-scale testing of stone arch bridges", *Computers and Structures*, 79(29-30), 2645-2662, https://doi.org/10.1016/S0045-7949(01)00109-2.

Ferrero, C., Calderini, C., Portioli, F. and Roca, P. (2021). "Large displacement analysis of dry-joint masonry arches subject to inclined support movements", *Engineering Structures*, 238, 112244, https://doi.org/10.1016/j.engstruct.2021.112244.

Gaetani, A., Bianchini, N. and Lourenço, P.B. (2021). "Simplified micro-modelling of masonry cross vaults: stereotomy and interface issues, *International Journal of Masonry Research and Innovation*, 6(1), 97-125, http://doi.org/10.1504/IJMRI.2021.112076.

Gönen, S. and Soyöz, S. (2022). "Reliability-based seismic performance of masonry arch bridges", *Structure and Infrastructure Engineering*, 18(12), 1658-1673, https://doi.org/10.1080/15732479.2021.1918726.

Güllü, H. and Özel, F. (2020). "Micro tremor measurements and 3D dynamic soil-structure interaction analysis for a historical masonry arch bridge under the effects of near-and far-fault earthquakes", *Environmental Earth Sciences*, 79, 1-29, https://link.springer.com/article/10.1007/s12665-020-09086-0.

Jindal, A., RN, G.D., Kumar, P., Kumar, V. and Rana, D. (2023). "Rehabilitation prospects of concrete pavements with self-compacting concrete containing wollastonite micro-fiber." *Civil Engineering Infrastructures Journal* 56(2), 221-233, https://doi.org/10.22059/CEIJ.2023.341456.1828.

Kassem, M.M., Nazri, F.M., Farsangi, E.N. and Ozturk, B. (2022). "Development of a uniform seismic vulnerability index framework for reinforced concrete building typology", *Journal of Building Engineering*, 47, 103838, https://doi.org/10.1016/j.jobe.2021.103838.

Korbar, T., Markušić, S., Stanko, D. and Penava, D. (2021). "Petrinja M6.2 earthquakes in 2020 damaged also solid linear infrastructure: are there similar active faults in Croatia", *1st Croatian Conference on Earthquake Engineering*, March 2021, http://doi.org/10.5592/CO/1CroCEE.2021.253.

Martinelli, P., Galli, A., Barazzetti, L., Colombo, M., Felicetti, R., Previtali, M., Roncoroni, F., Scola, M. and di Prisco, M. (2018). "Bearing capacity assessment of a 14th century arch bridge in Lecco (Italy)", *International Journal of Architectural Heritage*, 12(2), 237-256, http://doi.org/10.1080/15583058.2017.1399482.

Miranda, E., Brzev, S., Bijelic, N., Arbanas, Ž., Bartolac, M., Jagodnik, V., Lazarević, D., Mihalić Arbanas, S., Zlatović, S., Acosta Vera, A., Archbold, J., Bantis, J., Blagojevic, N.,

Borozan, J., Božulić, I., Cruz, C., Dávalos, H., Fischer, E., Gunay, S., Hadzima-Nyarko, M., Heresi, P., Lignos, T., Lin, T., Marinkovic, M., Messina, A., Miranda, S., Poulos, A., Scagliotti, G., Tomac, I., Tomic, I, Ziotopoulou, K., Žugić, Z. and Robertson, I. (2021). *Petrinja, Croatia December 29, 2020*, MW 6.4 Earthquake Joint Reconnaissance Report (JRR), https://doi.org/10.17603/ds2-1w0y-5080.

Mokrini, F., Waeyenberge, L., Viaene, N. and Moens, M. (2012). "First report of the cereal cyst nematode Heterodera latipons on wheat in Morocco", *Plant Disease*, 96(5), 774, https://doi.org/10.1094/PDIS-11-11-0999-PDN.

Novak, M.S., Uros, M., Atalic, J., Herak, M., Demsic, M., Banicek, M., Lazarevic, D., Bijelic, N., Crnogorac, M. and Todoric, M. (2020). "Zagreb earthquake of 22 March 2020-preliminary report on seismologic aspects and damage to buildings", *Gradevinar*, 72, 843-867, https://doi.org/10.14256/JCE.2966.2020.

Pelà, L., Aprile, A. and Benedetti, A. (2013). "Comparison of seismic assessment procedures for masonry arch bridges", *Construction and Building Materials*, 38, 381-394, https://doi.org/10.1016/j.conbuildmat.2012.08.046.

Pepi, C., Cavalagli, N., Gusella, V. and Gioffrè, M. (2021). "An integrated approach for the numerical modeling of severely damaged historic structures: Application to a masonry bridge", *Advances in Engineering Software*, 151, 102935, https://doi.org/10.1016/j.advengsoft.2020.102935.

Perković, N., Stepinac, M., Rajčić, V. and Barbalić, J. (2021). "Assessment of timber roof structures before and after earthquakes", *Buildings*, 11(11), 528, https://doi.org/10.3390/buildings11110528.

Samadi, D., Taghaddos, H., Nili, M.H. and Noghabaei, M. (2021). "development of a bridge maintenance system using bridge information modelling", *Civil Engineering Infrastructures Journal*, 54(2), 351-364, https://doi.org/10.22059/CEIJ.2020.298837.1661.

Seker, B.S., Cakir, F., Dogangun, A. and Uysal, H. (2014). "Investigation of the structural performance of a masonry domed mosque by experimental tests and numerical analysis", *Earthquakes and Structures*, 6(4), 335-350, https://doi.org/10.12989/eas.2014.6.4.335.

Stockdale, G., Milani, G. and Sarhosis, V. (2019). "Increase in seismic resistance for a full-scale dry stack masonry arch subjected to hinge control", *Key Engineering Materials*, 817, 221-228, https://doi.org/10.4028/www.scientific.net/KEM.817.221.

Valente, M. and Milani, G. (2019a). "Damage survey, simplified assessment and advanced seismic analyses of two masonry churches after the 2012 Emilia earthquake", *International Journal of Architectural Heritage*, 13(6), 901-924, https://doi.org/10.1080/15583058.2018.1492646.